Journal of Alloys and Compounds 509 (2011) 6819–6823

Contents lists available at ScienceDirect

Journal of Alloys and Compounds

journal homepage: www.elsevier.com/locate/jallcom

Synthesis, vacuum sintering and dielectric characterization of zirconia (t-ZrO_2) nanopowder

R. Pazhani [a], H. Padma Kumar [b], Angeo Varghese [c], A. Moses Ezhil Raj [d], Sam Solomon [e], J.K. Thomas [a,*]

[a] Electronic Materials Research Laboratory, Department of Physics, Mar Ivanios College, Nalanchira, Thiruvananthapuram 695015, Kerala, India
[b] Department of Physics, W.M.O. Arts and Science College, Muttil 673122, Wayanad, Kerala, India
[c] Mar Baselios College of Engineering & Technology, Thiruvananthapuram 695015, Kerala, India
[d] Department of Physics, Scott Christian College, Nagercoil 629003, Tamil Nadu, India
[e] Department of Physics, St. John's College, Anchal 691306, Kollam, Kerala, India

ARTICLE INFO

Article history:
Received 30 November 2010
Accepted 15 March 2011
Available online 22 March 2011

Keywords:
t-ZrO_2
Combustion synthesis
X-ray diffraction
TEM
Dielectrics

ABSTRACT

Phase pure zirconium oxide powders have been synthesized using the single step auto-ignition combustion method, the particles were nanometer sized (20 nm) and the size distribution was very narrow (3.4 nm). Systematic structural characterization revealed the t-ZrO_2 and indexed for its tetragonal structure (a = 3.5975 Å and c = 5.1649 Å). Calculated microstrain in most of the plane indicated the presence of compressive stress (65–288 MPa) along various planes of the particles. Observed space group ($P4_2/nmc$) revealed the presence of cations in the 8e positions (0.75, 0.25, 0.75) and the anions in the 16 h positions (0.25, 0.25, 0.4534). The metal-oxide (Zr–O) band observed at the low wavenumber region further confirmed the phase purity of the as-prepared ZrO_2 nanopowders. Peaks at the binding energy positions 2.042 and 0.525 keV in the energy dispersive X-ray spectrum revealed oxygen deficient zirconia. The particle size estimated by TEM was in good agreement with the results obtained through X-ray line broadening (20.81 nm) measurements. The nanopowders were sintered to above 98% of the theoretical density by using vacuum sintering technique at a relatively low temperature of 1300 °C. Stable tetragonal ZrO_2 experimentally yield the permittivity value of about 28 at 10 MHz.

1. Introduction

Zirconium oxide (ZrO_2) exhibiting high refractive index (2.17) and high optical transparency (E_g = 5.2 eV) in the UV–Vis–IR has instrumental in device fabrication in photonics [1]. In addition, zirconia has unique combination of electronic and mechanical properties that led to wide applications, as a structural material, solid-state electrolyte, catalyst and thermal barrier coatings [2]. ZrO_2 exists in three different phases namely room temperature stable monoclinic phase and high temperature stable tetragonal and cubic phases (metastable phases at room temperature). The metastable phase of zirconia (t-ZrO_2) is the focus of recent investigations due to their high hardness, chemical inertness and optical properties (Abbe number ≈ 35) make them important target materials for the fabrication of metal-halide lamps, solid state lasers, scintillators and bar-code scanners [3–6]. Recently, t-ZrO_2 has been proved to be a highly luminescent material, which is photochemically stable with low phonon energy (470 cm^{-1}) [7].

Such a technologically important zirconia nanostructure has been synthesized by different methods which include various wet-chemical processes [8], mechanochemical processing [9], salt-assisted aerosol decompositions [10], emulsion precipitation [11] and few more. Among the various wet-chemical processes, recently the combustion synthesis has attracted much attention due to its relatively low cost and better control of stoichiometry in comparison to other methods. The process basically involves the preparation of homogeneous fuel-oxidant precursor and subsequent combustion of an aqueous solution containing salts of the desired metals (usually nitrates) and some organic fuel, such as citric acid, urea, glycine, etc. [12–14]. Phase purity and characteristics of the combustion-synthesized powder are primarily depending on certain parameters; redox reaction between nitrate ions and the fuel, amount of the fuel used in the process, the enthalpy of combustion, amount of gas evolution and the rate of combustion [15,16]. In addition, fast decomposition rate, evolution of high volume of gaseous products and sufficient enthalpy of combustion yield nanocrystalline particles after calcination.

Few reports have been involved in the combustion synthesis of ZrO_2 nanocrystals by using various fuels. However, present article highlights the modified single step auto-igniting combustion synthesis of zirconia using citric acid as the fuel, since it has good

* Corresponding author. Tel.: +91 9447205190; fax: +91 471 2530887.
E-mail address: jkthomasemrl@gmail.com (J.K. Thomas).

0925-8388/$ – see front matter © 2011 Elsevier B.V. All rights reserved.
doi:10.1016/j.jallcom.2011.03.089

complexing ability, low ignition temperature (200–250 °C) and controlled combustion reaction with starting precursors [17]. In the present article we report the synthesis, structural, surface morphological, vacuum sintering and dielectric studies on the optimized single phase pure zirconia nanopowders.

2. Materials and methods

In modified single step auto-igniting combustion synthesis, an aqueous solution containing Zr^{2+} was prepared by dissolving typical amount of high purity $ZrOCl_2{\cdot}8H_2O$ in distilled water (~200 ml) in a glass beaker. Citric acid was then added as fuel and the oxidant/fuel ratio of the system was adjusted by adding nitric acid and ammonium hydroxide. Amount of citric acid was calculated based on total valence of the oxidizing and reducing agents for maximum release of energy during combustion. The resulting translucent solution was heated on a hot plate (at about 200 ± 250 °C) until it turned into a viscous solution. The solution boils upon heating and undergoes dehydration accompanied by foam. On heating further, the foam ignites by itself due to persistent heating giving a voluminous and fluffy product from combustion. The combustion product was subsequently characterized as single phase nanocrystals of ZrO_2. Grey ashes obtained after combustion were then collected for structural characterization and other morphological studies.

X-ray diffraction (XRD) data collection on the combustion-synthesized powder was carried out for phase identification and crystallite size determination using a Bruker D-8 X-ray diffractometer (CuKα radiation, Ni-filter). The powder-XRD data were collected in the 2θ range of 20–90°, in step scan mode with step width 0.02 and step time 2.40 s. The metal-oxide phase formation was identified from the recorded Fourier Transform Infrared(FTIR) spectrum in the range 400–4000 cm^{-1} (Thermo Nicolet Avtar 370 DTGS). The purity and the stoichiometry of the prepared sample were identified from the recorded EDAX spectrum using JEOL-6400 electron microscope operating at 20 kV. The sample was dusted on an adhesive conductive carbon disc attached to a mount and coated with a gold film prior to examination. The particle size and the morphology were recorded using Transmission Electron Microscopy TEM (model: PHILIPS-CM 200, resolution 2.4 Å) operating at 200 kV. The sample for TEM analysis was prepared by ultrasonically dispersing the powder in methanol and allowing a drop to dry on a carbon-coated copper grid.

Vacuum sintering has been done on the pelletized nanopowders prepared under the optimized preparation conditions. The final sintered product was produced by the two-step sintering techniques – pre-sintering in hydrogen atmosphere (at 550 °C) to avoid agglomeration and final sintering by vacuum sintering. Proper care has been taken not to exceed the melting point of the sintered base material. Moreover, control over heating rate, time, temperature and atmosphere has been taken into consideration to have reproducible results. Initially the pellets were heated in hydrogen ambient and then it was transferred to the vacuum furnace. In vacuum furnace the heat-treating process takes place inside an airtight vessel, where a vacuum is created. This helps to alleviate surface reactions. Furnace has high temperature refractory lining (Alumina–silica) to hold the process material and hold in the heat without breaking down during the several hours that they usually run. The heater arrangement optimizes temperature uniformity within the furnace hot zone. Indirect heating electrical resistance coils are used to heat the pellets placed inside a pre-evacuated sealed silica crucible at vacuum $p < 13$ Pa (10^{-1} mm/Hg). In the present study, heating rate was maintained at 10 °C/min and after attaining the predefined sintering temperature (1300 °C), the sample was heated continuously for a sintering time of 3 h. The sintered density was then calculated following Archimedes method.

The variation in the dielectric constant (ε_r) and loss factor ($\tan\delta$) of the sintered ZrO_2 have been studied using an Impedance Analyser (Agilent HP 4192A) in the frequency range 10KHz–10 MHz at room temperature.

3. Results and discussions

Fig. 1 shows the diffraction pattern of the as-prepared ZrO_2 powder sample. The crystallinity of the sample is evidenced by sharper diffraction peaks at respective diffraction angles which can be readily indexed for its tetragonal structure (t-ZrO_2). Obtained tetragonal phase is comparable with the standard JCPDS data (Card No. 81-1544) [18]. The sample exhibits only the tetragonal phase and the major peaks appears at $2\theta = 30.27°$, 35.23°, 50.27°, 60.18°, 62.95°, and 74.54°. It is further observed that there is no indication of low temperature monoclinic or the high temperature cubic phases. Evidence of the tetragonal symmetry might be again confirmed from the non-symmetric line shape around $2\theta = 35°$ and 60° regions of the XRD pattern. In the $2\theta = 35°$ region, the nonsymmetrical line shape originated from the splitting between the (0 0 2) and (1 1 0) peaks situated near by 2θ values 34.634° and 35.160° respectively. Similarly in the $2\theta = 60°$ region, non symmetrical peak shape is due

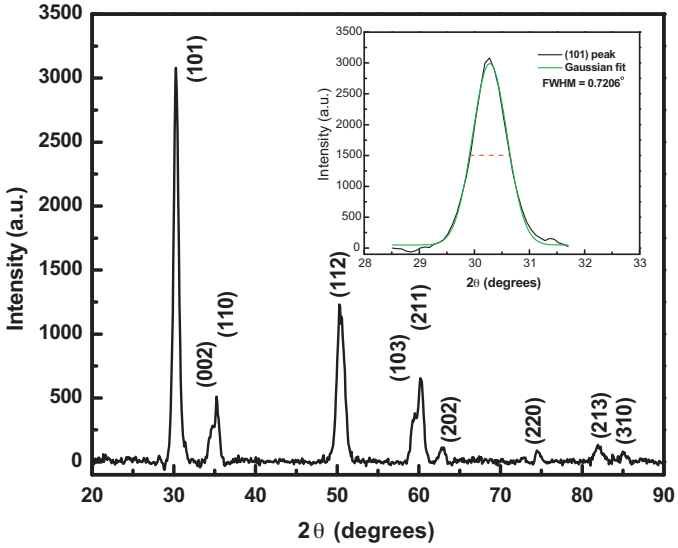

Fig. 1. XRD patterns of as-prepared ZrO_2 nanopowder sample. Inset shows the (1 0 1) predominant peak.

to the overlap of indexed peaks (1 0 3) and (2 1 1) situated respectively at $2\theta = 59.30°$ and 60.029°.

All the observed peaks in Fig. 1 are indexed assuming t-ZrO_2 polymorph (Table 1). This table gives a brief account of all the peaks about its position, Miller indices, interplanar distances (observed and standard), their deviations and the microstrain on the grains. The microstrain on the grains can be visualized from the line shifting in the XRD spectrum. It can be seen that the observed *d*-spacing of the diffraction planes are very close to the standard values and therefore the Δd_{hkl} values are very small in the order of 10^{-3} nm. The deviation in the *d*-spacing is the measure of line shifting which gives the value of microstrain in the nano powder sample. If d_0 is the observed *d*-spacing of the prepared sample and d_s, the spacing in the standard sample, the microstrain in the particles in the direction normal to the diffraction plane is $\Delta d_{hkl}/d_s$. If $d_0 > d_s$, then the microstrain is positive which indicates that the residual stress is tensile and if $d_0 < d_s$, microstrain is negative indicating generation of residual compressive stress in the surface. In the present study, calculated microstrain in most of the plane is negative, indicating the presence of compressive stress on the surface of the particles. Observed positive values of microstrain for the (0 2 2) and (1 0 3) planes may be due to induced error in the measurement of the 2θ value, since the respective peaks are nonsymmetrical.

The microstress present in the nanopowder sample can be defined as [19],

$$\sigma_{\text{stress}} = \frac{\varepsilon}{2}E \quad (1)$$

where *E* is the elastic constant or generally known as Young's modulus of the material. Young's modulus of zirconium oxide is 186.21 GPa [20] and therefore the compressive stress on the surface of the nanopowder is of the order 65–288 MPa along various planes of the particles.

Accurately measured d values for the (4 0 0) and (0 0 4) peaks are tabulated in Table 2. These values are again verified by use of the cell refinement software (Celcal) for the same tetragonal structure by considering all the indexed peaks. Obtained values $a = 3.5975$ Å and $c = 5.1649$ Å are consistent with the standard JCPDS values ($a = 3.6060$ Å, $c = 5.1758$ Å). Similarly, refined axial ratio c/a exactly matches with the standard value (Table 2) and is in agreement with the reported values. The calculated and refined values of unit cell volume of the crystal system also matches well with the standard values. Calculated and refined values of the density are

Table 1
Interplanar d_{hkl} spacings and microstrain in the t-ZrO_2 nanopowder.

Peak position 2θ (°)	(hkl)	Inter planar distance d_{hkl} (nm)		Deviation in d_{hkl} ($\Delta d_{hkl} = d_0 - d_s$) (nm)	Microstrain ($\varepsilon = \Delta d_{hkl}/d_s$)
		Observed (d_0)	Standard (d_s)		
30.2738	(1 0 1)	2.9499	2.9591	−0.0092	−0.0031
34.5578	(0 2 2)	2.5934	2.5879	0.0055	0.0021
35.2298	(1 1 0)	2.5454	2.5503	−0.0049	−0.0019
50.2658	(1 1 2)	1.8136	1.8164	−0.0028	−0.0015
59.1698	(1 0 3)	1.5602	1.5563	0.0039	0.0025
60.1778	(2 1 1)	1.5364	1.5399	−0.0035	−0.0023
62.9498	(2 0 2)	1.4753	1.4795	−0.0042	−0.0028
74.5418	(2 2 0)	1.2720	1.2751	−0.0031	−0.0024
81.7658	(2 1 3)	1.1769	1.1782	−0.0013	−0.0011
85.0418	(3 1 0)	1.1397	1.1405	−0.0008	−0.0007

listed in Table 2. The density of the powder sample is more than the standard value, implied that the prepared powder is compact and densely packed with few unit cells of the material. Moreover, from the observed space group ($P4_2/nmc$) and the reported data [21,22], it is assumed that the cations are located in the 8e position (0.75, 0.25, 0.75) and the anions are located in the 16h positions (0.25, 0.25, 0.4534).

The calculated crystallite size was about 20.81 nm, which reveals the nanocrystalline size of the prepared powder. From this value, the specific surface area was calculated on assuming the presence of spherical particles, by using the relation [13]:

$$S = \frac{6}{\rho D} \quad (2)$$

where ρ, the calculated density of the material and D, the particle size of the sample. The specific surface area is a dominant parameter in case of permeability and in the transport of a species that can adsorb on the mineral surfaces. The specific surface area of the spherical particles of the synthesized powder sample is 47 m^2/g. In general, decreased crystallinity with improvement in specific surface area leads to higher reaction rate. From the observed value, prepared material can be engaged in catalytic reactions.

In other combustion processes reported for the preparation of nanocrystals of some ceramic oxides, polyvinyl alcohol and urea were used as chelating agents and fuel, respectively and in all these cases phase pure powder was obtained only after high temperature calcination [23,24]. But in the present modified single step auto-ignition combustion method, citric acid was used as the chelating agent instead of polyvinyl alcohol and urea was replaced with ammonia. By changing the complexing agent and oxidant fuel system it was possible to get a single phase ZrO_2 as nanocrystals in a single step combustion.

FTIR spectrum of the ZrO_2 nano powder synthesized at the optimized preparation condition is shown in Fig. 2. For ZrO_2 nano crystals, three intense peaks centered at 420, 513, 758 cm^{-1} were observed, which is the characteristic band of the tetragonal ZrO_2 phase [25]. According to the available reports, observed bands at 420 and 513 cm^{-1} are attributed to the Zr–O stretching in tetragonal ZrO_2 [26,28]. Also the band at 758 cm^{-1} is the characteristic of Zr–O bending vibrations of ZrO_2 in ZrO_δ, usually $\delta = 4$ and 6, polyhedron [27,28]. Significantly all the above said bands have been reported in m-ZrO_2 [28]. The broad characteristic band at 513 cm^{-1} appears in t-ZrO_2 while at 628 cm^{-1} in c-ZrO_2 [27,28]. In general, all the four ZrO_2 polymorphs have very similar vibrational structures. A minor variation in their frequencies or relative intensities occurs in different Zr^{4+} distribution in the interstitial sites. They are sensitive to the oxygen vacancies and other defects [29].

Table 2
Unit cell parameters of the as-prepared ZrO_2 powder.

Unit cell parameters	Calculated	JCPDS standard	Cell refinement
Unit cell edge			
a (Å)	3.5849	3.6067	3.5975
Unit cell edge			
c (Å)	5.1919	5.1758	5.1649
Axial ratio c/a	1.448	1.435	1.436
Volume $V = a^2c$ (Å^3)	66.7237	67.3283	66.8442
Density (gm cm^{-3})	6.1311	6.0760	6.1200

These results reveal that the phase formation is complete for the as-prepared ZrO_2 nanopowder and there is no evidence for the presence of any organic intermediates in the sample. However, the observed weak bands at 3445 and 1587 cm^{-1} can be assigned to the stretching and bending vibrations of the O–H bands that reveal the presence of surface hydration.

The chemical composition of the ZrO_2 nanopowders prepared at the optimized condition was extracted from the energy dispersive X-ray spectrum (EDAX) which is shown in Fig. 3. The different elements of the spectrum are distinguished by different pulse amplitude produced in the detector proportional to the characteristic X-ray quantum energy. Peaks due to the presence of zirconium and oxygen appeared at the positions with the binding energy 2.042 and 0.525 keV respectively. The atomic percentages of the elements present in the prepared sample are respectively 74.45 and 25.55. EDAX result reveals oxygen deficient zirconia powders in the present conditions of preparation.

Numerous studies on nanocrystalline ZrO_2 have shown that pure metastable tetragonal and cubic phases can be stabilized at room temperature when the crystallite size is below a critical size primarily due to very high surface energy associated with it. When the crystallite size exceeds this size, the transformation of

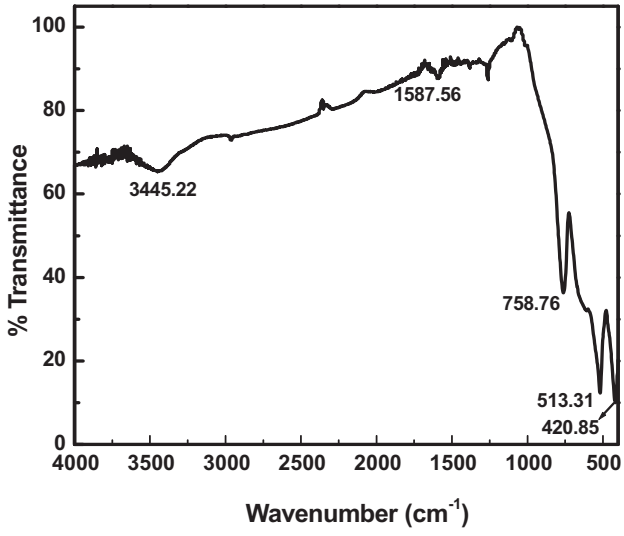

Fig. 2. FT-IR spectrum of as-prepared ZrO_2 nanocrystals.

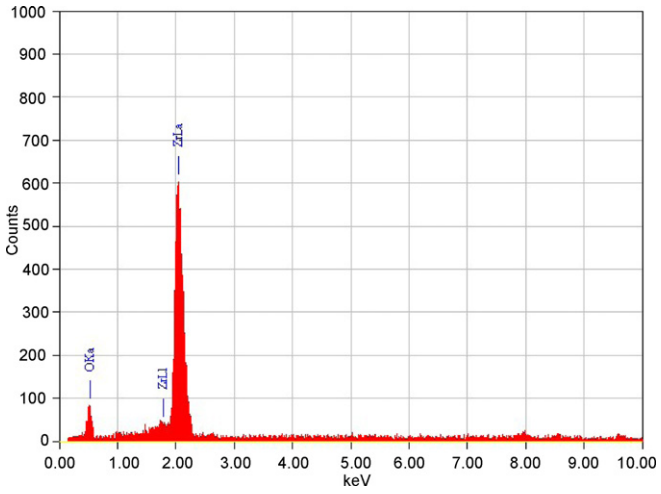

Fig. 3. Energy dispersive absorption X-ray spectrum of the as-prepared ZrO_2 nanocrystals.

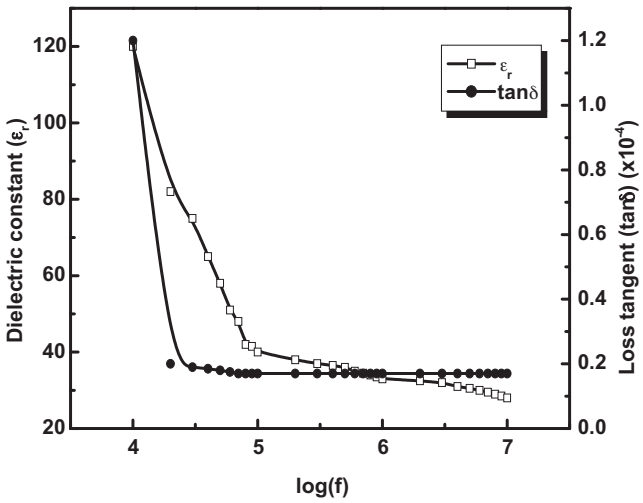

Fig. 5. Dielectric response of sintered ZrO_2.

metastable phases to the monoclinic one occurs due to decrease in surface energy [30,31]. Hence particle size analysis finds a place in deciding and transformation of crystalline phase.

Fig. 4 shows the TEM micrograph of as-prepared ZrO_2 powder, which reflects the highly agglomerated sub-micrometer powder having nearly spherical nanocrystals with facets of size around 20 nm. The crystallite size observed by TEM is in good agreement with the result estimated by X-ray line broadening (20.81 nm). The particle distribution is almost uniform and the deviation from the mean particle size is not exceeding 3.4 nm. The crystallite size obtained in the combustion-synthesized ZrO_2 powder seems to be above the critical size needed to stabilize the metastable cubic phase [32–34]. This study again favors for the evolution of tetragonal phase of the product for the present preparative conditions probably due to high degree of agglomeration which can reduce the surface energy. In addition, high enthalpy generated due to the fuel citric acid used for combustion also facilitates agglomeration.

In the present vacuum sintering technique, fully dense powder compacts were obtained with ultrafine and nano sized particles. Obtained density value 5.98 g/cc is in agreement with the JCPDS standard value of 6.076 g/cc, which is about 98.42% of the bulk value of the same material.

Fig. 5 shows the frequency dependence of dielectric constant and dielectric loss for the sintered ZrO_2 pellets. Measurements were carried out at various frequencies ranging from 10 kHz to 10 MHz at room temperature. As evidenced from the observed variations, the dielectric constant (ε_r) decreases as the frequency increases. At higher frequencies, the variations in ε_r almost ceases and attains a constant value of 28. This value of dielectric constant is comparable to the reported values [35,36]. However, dielectric constant of ZrO_2 and few of its solid solutions have been reported in the literature, and among these there is a considerable spread in values for nominally similar materials. Thus different sources give the permittivity for the same material varying by up to a factor of two; for example, for calcium-stabilized zirconia has been reported as being 16 or 26, and for monoclinic zirconia values are quoted from 13.5 to 24 [36]. The inconsistency in the observed values of permittivity may be due the measurement techniques used and also due the available crystalline phases of ZrO_2. Zirconia has a monoclinic unit cell at room temperature, but the added cations stabilize a higher symmetry tetragonal or cubic unit cell with corresponding changes in lattice parameters. This in turn alter the material properties specifically the dielectric constant. Present study deals mainly the stable tetragonal ZrO_2, which experimentally yield the permittivity value of about 28 at the frequency of 10 MHz. Fig. 5 shows the loss tangent variation with respect to the applied frequency in kHz to MHz range. The dielectric loss is about 1.2 at 10 kHz, which is comparatively higher than that observed at the MHz range. Observed higher loss in the low frequency region may be due to a high defect charge density existing in the material, which would lead to the loss of leakage conductance. At 10 MHz, the observed dielectric loss is only 0.17 and therefore zirconia can be used as dielectric resonators applicable to both terrestrial and satellite communications.

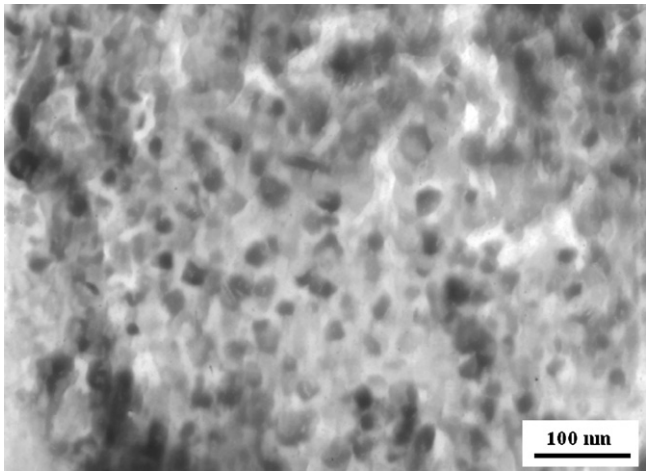

Fig. 4. TEM micro image of the as-prepared ZrO_2 nanopowder.

4. Conclusion

A simple, cost-effective and time-saving low-temperature single step auto igniting combustion synthesis has been developed to obtain nanocrystalline t-ZrO_2 powder. XRD results revealed the tetragonal phase with nano sized particles. The phase confirmation and the elemental analysis have been performed to judge the purity and stoichiometry of the prepared nanopowders. TEM image shows that the particle size is uniform and is around 20 nm. The vacuum sintered sample shows high sintered density of about 98% of the theoretical density at a relatively low temperature of 1300 °C. A high permittivity of about 28 is obtained at higher frequencies (10 MHz). The nanocrystalline ZrO_2 has the advantage of lower sintering temperature and better microwave

dielectric properties than that prepared by conventional techniques.

Acknowledgements

Author Dr. J.K. Thomas, acknowledges the financial assistance from Kerala State Council for Science Technology and Environment, Government of Kerala, Trivandrum 695004, India.

References

[1] A. Emeline, G.V. Kataeva, A.S. Litke, A.V. Panasuk, V.K. Ryabchuk, N.V. Sheremetyeva, N. Serpone, J. Phys. Chem. B 109 (2005) 5175–5185.
[2] T. Ma, Y. Huang, J. Yang, J. He, L. Zhao, Mater. Des. 25 (2004) 515–519.
[3] A. Rosenflanz, M. Frey, B. Endres, T. Anderson, E. Richards, C. Schardt, Nature 430 (2004) 761–763.
[4] Y. Rabinovitch, D. Tetard, M.D. Faucher, M. Pham-Thi, Opt. Mater. 24 (2003) 345–351.
[5] J. Li, Y. Wu, Y. Pan, J. Guo, J. Non-Cryst. Solids 352 (2006) 2404–2407.
[6] G. Chen, J. Johnson, S. Schweizer, J. Woodford, P. Newman, D. MacFarlane, Proc. SPIE-Int. Soc. Opt. Eng. 6142 (2006) 61422X/1.
[7] R. Reisfeld, M. Zelner, A. Patra, J. Alloys Compd. 300–301 (2000) 147–151.
[8] A. Cabanas, J.A. Darr, E. Lester, M. Poliakoff, J. Mater. Chem. 11 (2001) 561–568.
[9] P.G. McCormick, T. Tsuzuki, J.S. Robinson, J. Ding, Adv. Mater. 13 (2001) 1008–1010.
[10] B. Xia, I.W. Lenggoro, K. Okuyama, Adv. Mater. 13 (2001) 1579–1582.
[11] F.C.M. Woudenberg, W.F.C. Sager, N.G.M. Sibelt, H. Verweij, Adv. Mater. 13 (2001) 514–516.
[12] J. Schäfer, W. Sigmund, S. Roy, F. Aldinger, J. Mater. Res. 12 (1997) 2518–2521.
[13] R.E. Juárez, D.G. Lamas, G.E. Lascalea, N.E. Walsöe de Reca, J. Eur. Ceram. Soc. 20 (2000) 133–138.
[14] L.A. Chick, L.R. Pederson, G.D. Maupin, J.L. Bates, L.E. Thomas, G.J. Exarhos, Mater. Lett. 10 (1990) 6–12.
[15] R.D. Purohit, A.K. Tyagi, J. Mater. Chem. 12 (2002) 1218–1221.
[16] R.D. Purohit, B.P. Sharma, K.T. Pillai, A.K. Tyagi, Mater. Res. Bull. 36 (2001) 2711–2721.
[17] K. Zupan, S. Pejovnik, J. Macek, Acta Chim. Slov. 48 (2001) 137–145.
[18] Joint Commission of Powder Diffraction Data Files, PCPDFWIN, Version 1.30, Pennsylvania (1997).
[19] D.R. Lide (Ed.), CRC Handbook of Chemistry and Physics, CRC Press, Boca Raton, FL, 2005.
[20] R.S. Lima, A. Kucuk, C.C. Berndt, Surf. Coat. Technol. 135 (2001) 166–172.
[21] A. Bonamartini, F. Bondioli, A.M. Ferrari, Chem. Mater. 13 (2001) 4550–4554.
[22] H. Klug, L. Alexander, X-ray Diffraction Procedures for Polycrystalline and Amorphous Materials, John Wiley and Sons, New York, 1974.
[23] R.C. Patil, S. Radhakrishnan, K. Sushama Pethkar, Vijaymohanan, J. Mater. Res. 16 (2001) 1982–1988.
[24] S.K. Saha, Nanostruct. Mater. 8 (1997) 29–36.
[25] G. Štefanić, S. Musić, S. Popović, A. Sekulić, J. Mol. Struct. 408/409 (1997) 391–394.
[26] G. Stefanic, I.I. Stefanic, S. Music, Mater. Chem. Phys. 65 (2000) 197–207.
[27] A. Feinberg, C.H. Perry, J. Phys. Chem. Solids 42 (1981) 513–518.
[28] T. Hirata, E. Asari, M. Kitajima, J. Solid State Chem. 110 (1994) 201–207.
[29] A. Mondal, S. Ram, Ceram. Int. 30 (2004) 239–249.
[30] Y. Murase, E. Kato, J. Am Ceram. Soc. 66 (1983) 196–200.
[31] R.C. Garvie, J. Phys. Chem. 69 (1965) 1238–1243.
[32] A. Clearfield, Inorg. Chem. 3 (1964) 146–148.
[33] K.S. Mazdiyasni, C.T. Lynch, J.S. Smith, J. Am. Ceram. Soc. 49 (1966) 286–287.
[34] S. Roy, J. Ghose, Mater. Res. Bull. 35 (2000) 1195–1203.
[35] J. Koo, Y. Kim, H. Jeon, Jpn. J. Appl. Phys. 41 (2002) 3043–3046.
[36] D.P. Thompson, A.M. Dickins, J.S. Thorp, J. Mater. Sci. 27 (1992) 2267–2271.